JASA ARTICLE

Influence of level difference due to vocal folds angular asymmetry on auto-oscillating replicas

Anne Bouvet,[1] Isao Tokuda,[2] Xavier Pelorson,[1] and Annemie Van Hirtum[1,a)]
[1]*LEGI, UMR CNRS 5519, Grenoble Alpes University, France*
[2]*Department of Mechanical Engineering, Ritsumeikan University, Nojihigashi, Kusatsu, Shiga 525-8577, Japan*

ABSTRACT:
Dysphonia is often caused by level difference between left and right vocal folds, which are positioned on different angles with respect to the transverse plane, resulting in angular asymmetry. Unilateral vocal fold paralysis may cause such angular asymmetry. In this case, the normal vocal fold is located on the transverse plane, whereas the paralyzed vocal fold is rotated in the sagittal plane as its posterior edge is moved up to the superior direction. The effect of such angular asymmetry (up to 25°) between the left and right vocal fold on the auto-oscillation is experimentally studied using mechanical replicas. For all replicas, it is observed that, as full contact between vocal folds is lost, increase of angular asymmetry results in a decrease of the signal-to-noise ratio, an increase of the total harmonic distortion rate, and an increase of the oscillation threshold pressure. These general tendencies are in agreement with clinical findings reported for vertical level difference during phonation. In analogy to the preceding experimental study in which vocal folds are spaced in parallel with a vertical trade-off, a formula is proposed to describe the oscillation threshold as a function of angular asymmetry. © *2020 Acoustical Society of America*.
https://doi.org/10.1121/10.0000742
(Received 11 July 2019; revised 16 January 2020; accepted 28 January 2020; published online 18 February 2020)
[Editor: Zhaoyan Zhang] Pages: 1136–1145

I. INTRODUCTION

Vocal folds (VF) asymmetry is reported as one of the main causes of glottic insufficiency resulting in dysphonia.[1] Glottic insufficiency is often caused by complete or partial VF paralysis, such as unilateral vocal fold paralysis (UVFP). UVFP has many causes and is characterized by vocal fatigue and a breathy voice.[1]

Clinical examinations show that UVFP introduces left-right asymmetries to the shape, tension, and positioning of the VFs. Videostroboscopic imaging (Fig. 1) reveals that asymmetrical positioning of the VFs in the sagittal plane prevents complete glottal closure,[1–3] which is suggested to be the main physical cause of the observed breathy voice. The VF positioning asymmetry results from both the normal and paralyzed VFs. In order to compensate for the reduced movement of the paralyzed VF, the position of the normal VF in the inferior-superior direction is changed. Consequently, a vertical level difference between the left and right VF emerges, where the paralyzed VF is often inclined in the sagittal plane (right VF in Fig. 1) and the normal VF remains in the transverse plane (left VF in Fig. 1) as described in the literature.[3–5] Quantitative characterization of this spatial asymmetry from imaging on human subjects is extremely tedious.[1–3] Nevertheless, the vertical level difference during phonation is reported[3] to yield several millimeters (i.e., 1.3 ± 1.5 mm or up to 3 mm) for UVFP subjects. The effect of positioning asymmetry on human vocalization cannot be studied independently from tension or shape asymmetry between left and right VFs. In that sense, physical studies of auto-oscillation using mechanical replicas are of interest when aiming at a systematic study of the influence of VF positioning asymmetry.

Recently,[4,5] the impact of parallel level difference between VFs, hereafter referred to as parallel level difference, was investigated. The preceding study, however, did not take into account the inclination of the paralyzed VF, which is physiologically closer to reality. Therefore, in this work, the influence of the inclination of one VF is studied (i.e., angular level difference). The normal VF is kept in its transverse plane, whereas the paralyzed VF is rotated in the sagittal plane so that its posterior edge is moved in the superior direction imposing a left-right VF asymmetry angle (α). Our aim is to systematically study the influence of asymmetry angle $\alpha > 0°$ on the auto-oscillation of mechanical replicas. Quantified objective oscillation features inform on the effect of α on the oscillation system (threshold pressures, oscillation frequency) as well as on overall spectral properties [signal-to-noise ratio (SNR), harmonic distortion rate] also used in voice quality studies.[13,14] There have been numerous studies on left-right asymmetry focusing on other VF properties such as tension and shape.[6–11] In the present study, symmetry of such properties is maintained so as to concentrate only on the angular asymmetry between left and right VFs.

In the next section (Sec. II), VF replicas are introduced, glottal replicas with left-right angular asymmetry are described, and mechanical resonances are characterized. Section III reports on experiments on fluid–structure

a)Electronic mail: annemie.vanhirtum@univ-grenoble-alpes.fr

 0001-4966/2020/147(2)/1136/10/$30.00

https://doi.org/10.1121/10.0000742

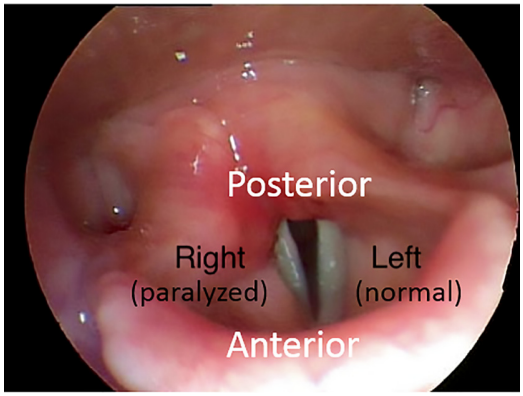

FIG. 1. (Color online) Videostroboscopic image of unilateral vocal fold paralysis. Adapted from Rosen and Simpson (Ref. 1) (page 29).

interaction and their results. To elucidate the oscillation onset pressure, an analogy of the angle asymmetry to parallel level difference is proposed in Sec. IV. The final section is devoted to conclusions and discussions.

II. REPLICAS

A. VFs replicas: M5, MRI, and EPI

Three deformable silicone VF replicas are used, labeled M5, MRI, and EPI, respectively. A medio-frontal and top view of symmetrically mounted VF replicas ($\alpha = 0°$) and layer thicknesses l_d are illustrated in Fig. 2. The three replicas differ due to their multi-layer composition as well as due to their geometry. In the next paragraphs, first the different layers are described, and next different casts are discussed.

Each silicone VF replica consists of an overlay of silicone molding layers obtained following the procedure detailed in literature.[4,15–17] Concretely, two (M5), three (MRI), and four layers (EPI) are superposed resulting in three different VF replicas, labeled M5, MRI, and EPI, respectively. The layers aim to reproduce the properties (Young's modulus $\mathcal{E}$, thickness l_d) of the different VF constituents for an adult male:[18–21] the thyroid muscle (vocalis), the superficial layer of the lamina propria (Reinke's space), the underlying ligament of the lamina propria without tension, and the epithelium. Each layer is composed as a mixture of silicone thinner and two parts of either A&B Ecoflex (03–00, Smooth-On, Inc., Easton, Pennsylvania) or two parts A&B DragonSkin (FX Pro, Smooth-On, Inc., Easton, Pennsylvania), labeled Ecoflex/Silicone (ES) and Dragon Skin/Silicone (DS), respectively. The mixing ratio $\mathcal{M}$ (ES or DS Part A: Part B: Silicone) differs between constituent layers as detailed in Table I. The properties (tensile tests, electromechanical press INSTRON 3369) of each layer are detailed in Table I. Note that the values of $\mathcal{E}$ are consistent with those reported in literature.[4,15–17]

The M5 VF replica is a two-layer model reproducing the muscle and superficial layer of the lamina propria (see Table I) molded with the cast shaped in accordance with the M5 geometry.[15,17,22] The MRI replica has a three-layer structure, obtained by adding a thin surface layer representing the epithelium to the two-layer structure of the M5 replica. This replica is molded using a realistic VF geometry cast obtained from magnetic resonance imaging. The MRI geometry adopts a trapezoidal shape in the transverse plane as seen from the top view in Fig. 2, whereas the M5 replica is rectangular. Therefore, the MRI shape is more complex than the M5 shape and more faithful to the shape of the human VF. Note that, compared to the MRI VF replicas reported in literature,[4,15,17] an epithelium layer is added in

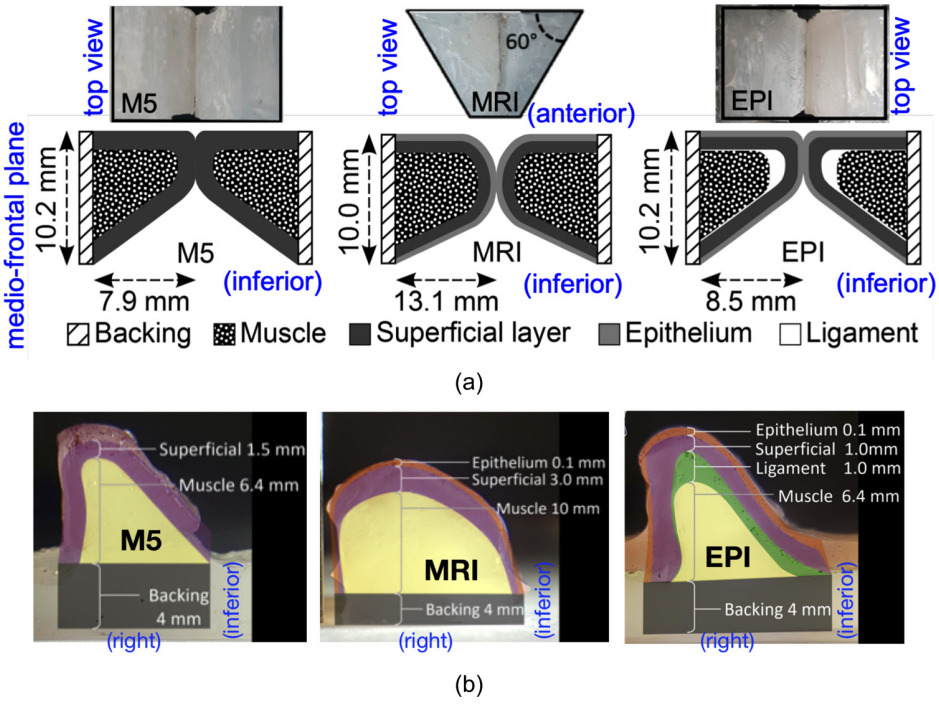

FIG. 2. (Color online) Symmetrically ($\alpha = 0°$) mounted vocal fold replicas M5, MRI, and EPI: (a) geometry, composition, and (b) layer thicknesses ld.

TABLE I. Layer properties in human (Refs. 18–21) and in silicone VF replicas (M5[a], MRI[b], EPI[c]): Young modulus $\mathcal{E}$, ecoflex-to-silicone ratio $\mathcal{M}$, layer thickness l_d. ES Ecoflex/Silicone mixture. DS Dragonskin/Silicone mixture.

	Male adult (Refs. 18–21)		VF replica		
Layer	$\mathcal{E}$ [kPa]	l_d [mm]	$\mathcal{E}$ [kPa]	$\mathcal{M}$ [-]	l_d [mm]
Muscle	18–23 ± 2.4	6.0	10.4[a] 4.9[b] 21.9[c]	ES 1:1:2[a] ES 1:1:4[b]ES 1:1:1[c]	6.4[a] 10.0[b] 6.4[c]
Ligament	30–36	0.8	4.9[c]	ES 1:1:4[c]	1.0[c]
Superficial	35–49 7.1	0.6	4.9[a] 0.2[b,c]	ES 1:1:4[a] ES 1:1:8[b,c]	1.5[a] 3.0[b] 1.0[c]
Epithelium	40–60	0.1	52[b,c]	DS 1:1:1[b,c]	0.1[b,c]

[a]M5: muscle and superficial
[b]MRI: muscle, superficial and epithelium
[c]EPI: muscle, ligament, superficial and epithelium

this work. The EPI replica is molded with the M5 cast as compared in Ref. 17. A four-layer structure is obtained by inserting an extremely soft ligament layer between the vocalis muscle and the superficial layer. An epithelium layer is added to the superficial layer. Each VF replica is mounted on a backing layer (DS, ratio $\mathcal{M}$ 1:1:1, thickness 4 mm) in order to attach it to a rigid support.

B. Glottal replicas with imposed asymmetry angle α

Each VF is placed in a rigid holder that is adapted to the M5, MRI, or EPI VF replica geometry. Dimensions are summarized in Table II and depicted in Fig. 3 with largest thickness E and smallest thickness e along the inferior-superior direction, and length L along the posterior-anterior direction. The right VF (normal) is fixed in the transverse plane, whereas the left VF (paralyzed) is rotated so that its posterior edge is lifted up in the superior direction resulting in the left-right VF asymmetry angle α shown in Fig. 3. For all glottal VF replicas, the rotation axis along the left-right direction is fixed in the rigid holder at $a = 4.5$ mm from the anterior edge (Table II).

Experiments are performed for 13 different values of left-right asymmetry angle α, ranging from $\alpha = 0^\circ$ up to $\alpha = 24.6^\circ$ affecting the glottal gap at rest. For symmetric angular configuration ($\alpha = 0^\circ$), the glottal gap area in the transverse plane is negligible as the VFs are in full contact (Fig. 2). When α is increased, air leakage occurs through a glottal gap in the medio-sagittal plane, since the VFs are no longer in full contact, as depicted in Fig. 3 (red dashed triangle). The triangular gap with area A, base l_A, and height h_A appears near the posterior VF edge and extends toward the anterior edge as α increases. In this sense, l_A indicates the glottal gap length in the posterior-anterior direction between the normal right VF and the paralyzed left VF. Note that $l_A > L$ can occur due to the position of the rotation axis at a distance $a > 0$ from the anterior VF edge, as shown in Fig. 3(b). The degree of VF's contact as a function of α is then expressed as $\mathcal{G} \in [0\ 1]$:

$$\mathcal{G}(\alpha) = \begin{cases} 0 & \text{if } \ l_A \geq L, \\ 1 - \dfrac{l_A(\alpha)}{L} & \text{otherwise.} \end{cases} \tag{1}$$

Three contact regimes (I, II, and III) are identified as α increases: I) $\mathcal{G} = 1$ when $l_A = 0$ (i.e., full VF's contact), II) $1 > \mathcal{G} > 0$ when $0 < l_A < L$ (i.e., partial VF's contact), and III) $\mathcal{G} = 0$ when $l_A \geq L$ (i.e., no VF contact). Note that full contact (regime I) implies no air leakage and hence $A = 0$, whereas, for $A > 0$, either partial contact (regime II) or no contact (regime III) occurs depending on α. Two critical angles $\alpha_{I,II}$ and $\alpha_{II,III}$ are then defined: $\alpha_{I,II}$ indicating the largest angle, for which full contact occurs (shift from regime I to II) and $\alpha_{II,III}$ indicating the largest angle, for which partial contact occurs (shift from regime II to III). Analytic expressions for glottal gap area $A(\alpha)$, its associated triangle base length $l_A(\alpha)$, and triangle height $h_A(\alpha)$ follow from trigonometric reasoning using geometrical VF replica parameters L, E, e, and a:

$$A(\alpha) = \begin{cases} 0 \quad \text{if} \quad \tan(\alpha)\left(L + a + \dfrac{E/2 - e}{\sin(\alpha)}\right) < \dfrac{E}{2}, \\ \dfrac{1}{2 \cdot \tan(\alpha)} \cdot \left(\left(L + a + \dfrac{1}{\sin(\alpha)} \cdot \left(\dfrac{E}{2} - e\right)\right) \cdot \tan(\alpha) - \dfrac{E}{2}\right)^2 \\ \quad + \dfrac{1}{2} \cdot \tan(\alpha) \cdot (E - e) \cdot \left(e - 2 \cdot \tan\left(\dfrac{\alpha}{2}\right) \cdot (L + a)\right) \quad \text{otherwise,} \end{cases} \tag{2}$$

and

JASA
https://doi.org/10.1121/10.0000742

TABLE II. Dimensional parameters (L, E, e, a) and critical asymmetry angles $\alpha_{(I,II),(II,III)}$ for all replicas (M5, MRI, and EPI).

Replica	L [mm]	E [mm]	e [mm]	a [mm]	$\alpha_{I,II}$ [°]	$\alpha_{II,III}$ [°]
M5	17.0	10.7	2.99	4.5	8.1	29.2
MRI	18.0	10.0	3.00	4.5	7.8	28.8
EPI	17.0	10.2	1.09	4.5	3.0	14.0

$$l_A(\alpha) = \begin{cases} 0 & \text{if } \tan(\alpha)\left(L + a + \dfrac{E/2 - e}{\sin(\alpha)}\right) < \dfrac{E}{2} \text{ or } A = 0, \\ 2\sqrt{\dfrac{A(\alpha)}{\sin(2\alpha)}} & \text{otherwise,} \end{cases} \tag{3}$$

so that h_A depicted in Fig. 3(b) varies as

$$h_A(\alpha) = \begin{cases} 0 & \text{if } l_A = 0, \\ \dfrac{2A(\alpha)}{l_A(\alpha)} & \text{otherwise,} \end{cases} \tag{4}$$

and thus ratio $(h_A/l_A)(\alpha) = 2A(\alpha)/l_A^2(\alpha)$.

For each replica (M5, MRI, and EPI), $\mathcal{G}(\alpha)$ [Eq. (1)], $A(\alpha)$ [Eq. (2)], and $h_A(\alpha)$ [Eq. (4)] are plotted in Fig. 4. The curves correspond to analytic expressions, while the symbols indicate asymmetry angles ($\alpha < 25°$) at which the experiments were carried out. Critical angles $\alpha_{I,II}$ and $\alpha_{II,III}$ are summarized in Table II and plotted (vertical annotated lines) in Fig. 4(a). Values of $\mathcal{G}(\alpha)$, $A(\alpha)$, and $\alpha_{(I,II),(II,III)}$ for M5 and MRI are close to each other, since their geometrical parameters (L, E, e, and a in Table II) are similar. For EPI, on the other hand, e yields about one-third of the value for M5 and MRI so that glottal gap $A(\alpha)$ increases more rapidly and VF's contact degree $\mathcal{G}(\alpha)$ reduces more rapidly than those of M5 and MRI. As a consequence, in the range of our study $\alpha < 25°$, all three contact regimes occur for EPI as $\alpha_{II,III}^{EPI} < 25°$ (Table II), whereas regime III (no contact, $\mathcal{G} = 0$) does not occur for M5 and MRI, since $\alpha_{II,III}^{MRI,M5} > 25°$ holds (Table II). Considering that initial pre-phonatory glottal gap area for healthy human speakers[23] yields less than 5 mm^2 [dashed horizontal line in Fig. 4(b)], it follows that the glottal gap area for $\alpha = 24.6°$ is increased by a factor of 8 (for M5) or more (for EPI and MRI). Height h_A [Fig. 4(c)] quantifies the maximum distance between both VFs along the inferior-superior direction and therefore provides a rough (since e is neglected) approximation for the vertical level difference measured during disordered human phonation[3] {i.e., 1.3 ± 1.5 or up to about 3 mm [dashed horizontal line in Fig. 4(c)]}. For $\alpha = 24.6°$, the height of $h_A \approx 6$ mm is twice as much as the value reported on humans. Thus, the range of asymmetry angle α studied in our experiments comprises the range observed for human phonation. Note that $h_A \leq 3$ mm corresponds to $\alpha \leq 13°$ for EPI and to $\alpha \leq 17°$

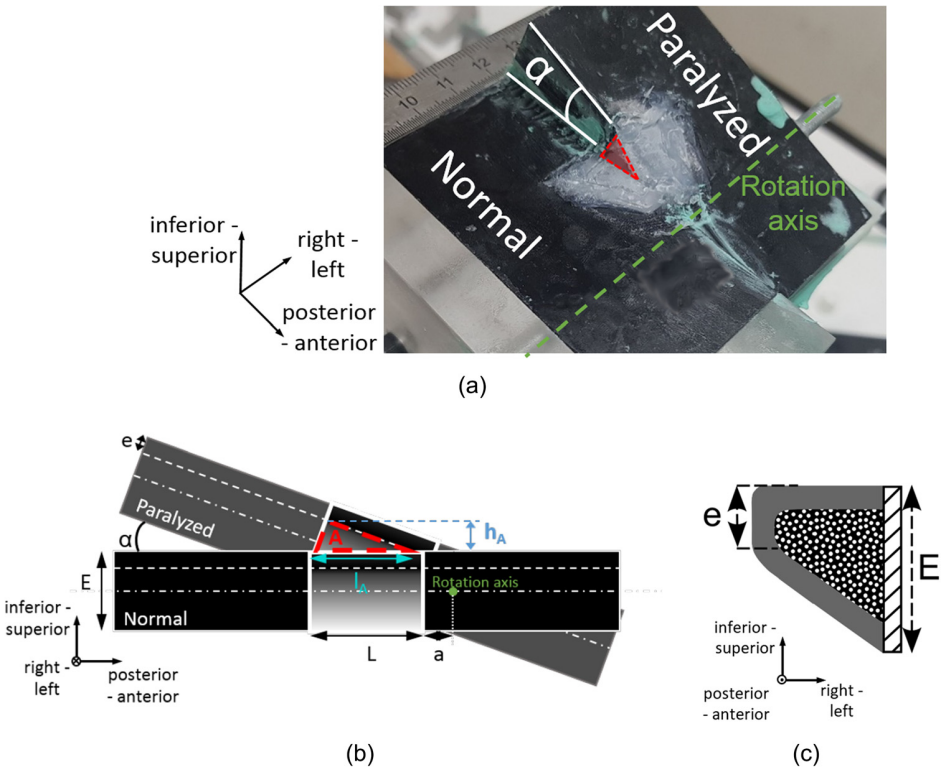

FIG. 3. (Color online) Imposed asymmetry angle α, glottal gap parameters A, lA, and hA and geometrical parameters E, e, L, and a: (a) glottal gap (red triangle) for MRI replica with $\alpha = 20°$ ($A \approx 32$ mm2, $l_A \approx 14.2$ mm and $h_A \approx 4.6$ mm), (b) sagittal view, (c) left vocal fold, (a) general superior view, MRI, (b) sagittal side view, (c) medio-frontal view.

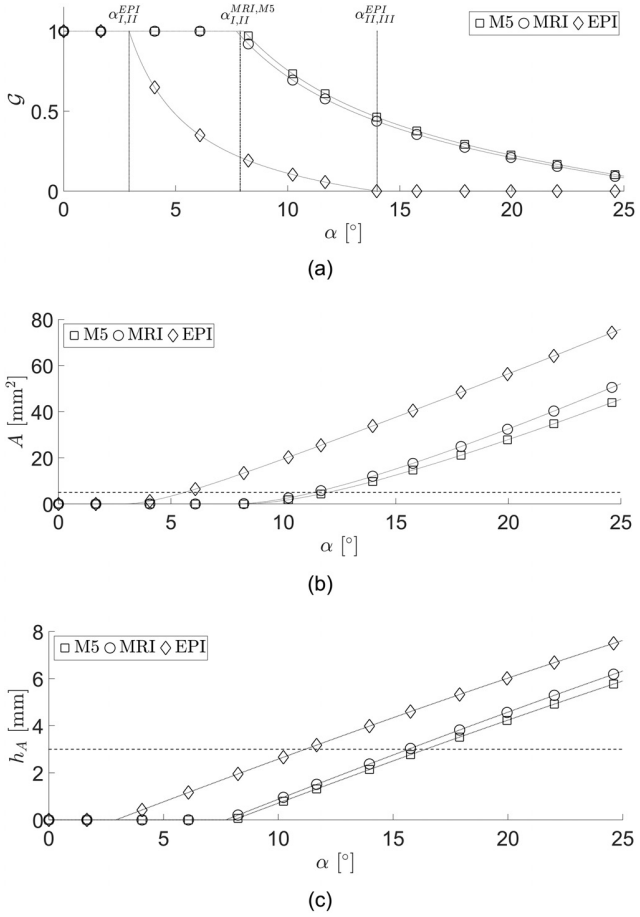

FIG. 4. Geometrical characterization of M5, MRI, and EPI replicas as a function of asymmetry angle α: (a) degree of contact $\mathcal{G}$ [Eq. (1)] and critical angles $\alpha_{(I,II),(II,III)}$ (vertical lines), (b) glottal gap area A [Eq. (2)] and reported maximum normal pre-phonatory glottal area (Ref. 23) (5 mm2, horizontal line), and (c) glottal gap height hA [Eq. (4)] and maximum vertical level difference reported during human phonation (Ref. 3) (3 mm, horizontal line). Symbols indicate experimentally assessed α values, (a) $\mathcal{G}(\alpha)$, (b) $\mathcal{A}(\alpha)$, (c) $h_A(\alpha)$.

for M5 and MRI. The ratio $(h_A/l_A)(\alpha)$ increases from 0 up to 0.4 for all replicas, indicating that the height h_A of the leakage triangle remains less than half of its base l_A for all α.

C. Mechanical characterization of replicas

Mechanical resonance properties of glottal replicas are examined for symmetric angular configuration ($\alpha = 0°$). A shaker (Modalshop K2007E) equipped with a mobile bar (length 230 mm and diameter 3.7 mm) is positioned so that the free bar end is in contact with the VF replica. Sinusoidal signals from 80 Hz to 350 Hz with a frequency step of 1 Hz and a duration of 1 s are fed to the shaker in order to excite the structure. An accelerometer (PCB 482A21) is attached to the mobile bar to measure the applied excitation $x(t)$. A laser (wavelength 635 nm) and photo-diode (BPW34) are aligned along the inferior and superior side of the replica, respectively. The response $y(t)$ of the replica to the excitation is then gathered from the photo-diode (BPW34) as the

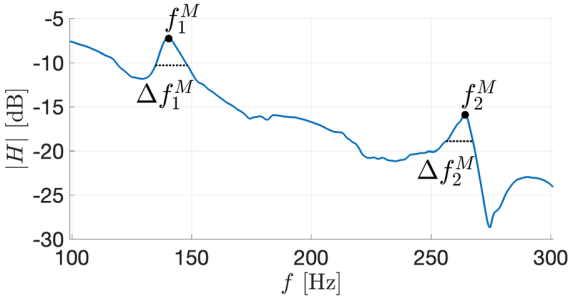

FIG. 5. (Color online) Estimated amplitude $|H(f)|$ for the EPI replica with $\alpha = 0°$ with resonance frequencies (f_1^M, f_2^M) and bandwidths (Δf_1^M, Δf_2^M).

amount of laser light modulated by the replica varies during excitation.

Frequency transfer functions $H(f) = X(f)/Y(f)$, representing the ratio of the *Fourier* transforms of response $X(f) = \mathcal{F}(x(t))$ to excitation $Y(f) = \mathcal{F}(y(t))$, are estimated in order to characterize the mechanical resonances. Frequency f^M associated with the maximum amplitude $|H(f)|$ and -3 dB frequency bandwidth Δf^M ($|H(f)| > |H(f^M)| - 3$ dB) are extracted. The resonance quality factor Q^M yields $Q^M = f^M/\Delta f^M$. The estimated amplitude $|H(f)|$ and the detected resonances for EPI are illustrated in Fig. 5. Mechanical resonance properties and standard deviations for all replicas (M5, MRI, and EPI) are summarized in Table III. For all replicas, two mechanical resonances are identified.

III. FLUID-STRUCTURE INTERACTION EXPERIMENTS

A. Experimental approach

In order to reproduce a fluid-structure interaction leading to auto-oscillation, glottal VF replicas are positioned vertically, as shown in Fig. 3(a). A rigid uniform tracheal tube (diameter 16 mm, length 460 mm, acoustic resonance frequency 185 Hz) is attached to the inferior end of the glottal VF replica. Continuous steady airflow (density $\rho_G = 1.2\,\mathrm{kg\cdot m^{-3}}$, dynamic viscosity $\mu_G = 1.8 \times 10^{-5}$ Pa·s, temperature 24±2 °C) is provided by an air compressor (Hitachi SC820) connected to a pressure reservoir (volume 0.04 m^3) to which the tracheal tube is mounted.[4] The transition is smoothed by a cone between the reservoir and the tracheal tube (section ratio 0.3). The pressure reservoir is filled with acoustic foam in order to avoid parasite acoustic resonances. The compressor is equipped with a pressure

TABLE III. Mechanical resonance properties (resonance frequencies $f_{1,2}^M$, bandwidths $\Delta f_{1,2}^M$, quality factor $Q_{1,2}^M$), and standard deviations of replicas for $\alpha = 0°$.

	first resonance peak			second resonance peak		
Replica	f_1^M [Hz]	Δf_1^M [Hz]	Q_1^M [-]	f_2^M [Hz]	Δf_2^M [Hz]	Q_2^M [-]
M5	142±3	16±7	10±5	264±3	9±3	29±2
MRI	144±2	13±4	11±3	262±2	8±2	32±5
EPI	141±2	13±2	11±2	264±2	15±6	21±9

https://doi.org/10.1121/10.0000742

regulator (10202 U, Fairchild, Winston-Salem, North Carolina). A pressure transducer (Kyowa PDS-70GA, accuracy ± 5 Pa) is positioned in a pressure tap in the tracheal wall, 185 mm upstream of the glottal VF replica, in order to measure upstream pressure P_u with sampling frequency $f_s = 10$ kHz.

For each VF replica, 13 different asymmetry angles $\alpha < 25^\circ$ are imposed as outlined in Section B, and a rigid uniform vocal tract tube of length 170 mm (diameter 16 mm, acoustic resonance frequency 500 Hz) can be attached airtight along the superior end of the VF replica. The effect of angular asymmetry α on the fluid-structure interaction is characterized by analyzing the measured upstream pressure $P_u(t)$. Upstream pressures associated with auto-oscillation onset (P_{On}) and offset (P_{Off}) are sought. Next, auto-oscillation features are analyzed for 5 s of steady-state upstream pressure signal $P_u(t)$, while the mean upstream pressure $\bar{P}_u \approx P_{On}$ holds, as illustrated in Fig. 6. The first harmonic (or fundamental) frequency f_0 is extracted. The second f_1 and third f_2 harmonic frequencies of f_0 are detected when its power (in dB) yields at least half the power of f_0. The harmonic contents of $P_u(t)$ are then further characterized by the total harmonic distortion rate (THD; in dB) computed as the ratio between the summed power of higher harmonic frequencies $\mathcal{P}_{harm}$ and the power of the first harmonic frequency $\mathcal{P}_{f_0}$:

$$\mathrm{THD} = 10\log_{10}\left(\frac{\mathcal{P}_{harm}}{\mathcal{P}_{f_0}}\right). \tag{5}$$

The power ratio $\mathcal{P}_{f_1}/\mathcal{P}_{f_0}$ between the second and first harmonics is quantified as well. Next, the SNR (in dB) is obtained as the ratio of the summed power of all signal harmonics $\mathcal{P}_{signal}$ based on the first harmonic frequency f_0 to the summed power of the remaining noise $\mathcal{P}_{noise}$:

$$\mathrm{SNR} = 10\log_{10}\left(\frac{\mathcal{P}_{signal}}{\mathcal{P}_{noise}}\right). \tag{6}$$

All experiments are repeated three times so that the average and standard deviation of the extracted features are plotted. Experiments are performed with and without a vocal tract tube. Since their resulting features are similar, only experimental results with a vocal tract tube are shown. It follows that the results are not much affected by acoustical coupling with the supraglottal vocal tract.

B. Experimental results

Oscillation onset (P_{On}) and offset (P_{Off}) pressures are plotted as a function of α in Fig. 7(c). Associated fundamental (f_0) frequencies and detected second (f_1) and third (f_2) harmonics are shown in Fig. 8. The minimum and maximum onset pressures $P_{On}(\alpha)$ relative to the value for symmetric angular configuration ($\alpha = 0^\circ$) are quantified in Table IV. The minimum of the onset pressure ($\min(P_{On}(\alpha))$) occurs for $\alpha > 0^\circ$: within regime I (full contact, $\mathcal{G} = 1$) for the MRI replica and within regime II (partial contact, $\mathcal{G} \in]0, 1[$) for the M5 and EPI replicas. This suggests that small values of α (under 10°) have a beneficial effect. Nevertheless, the amount of decrease is limited to less than 13% for all replicas and is very low for the MRI replica, which is the most realistic geometry compared to human VF. In addition, other quantities (SNR, THD, etc.) have to confirm this tendency.

The maximum of the onset pressure ($\max(P_{On}(\alpha))$) occurs near the largest asymmetry angle 24.6°, and the relative increase yields more than 29.5% for all replicas. For all replicas, the onset pressure increases for $\alpha \geq 15^\circ$. For $\alpha < 15^\circ$, the shape of the $P_{on}(\alpha)$ curve varies between replicas, because of its dependence on the detailed geometry and the layer composition of the individual replica. It is

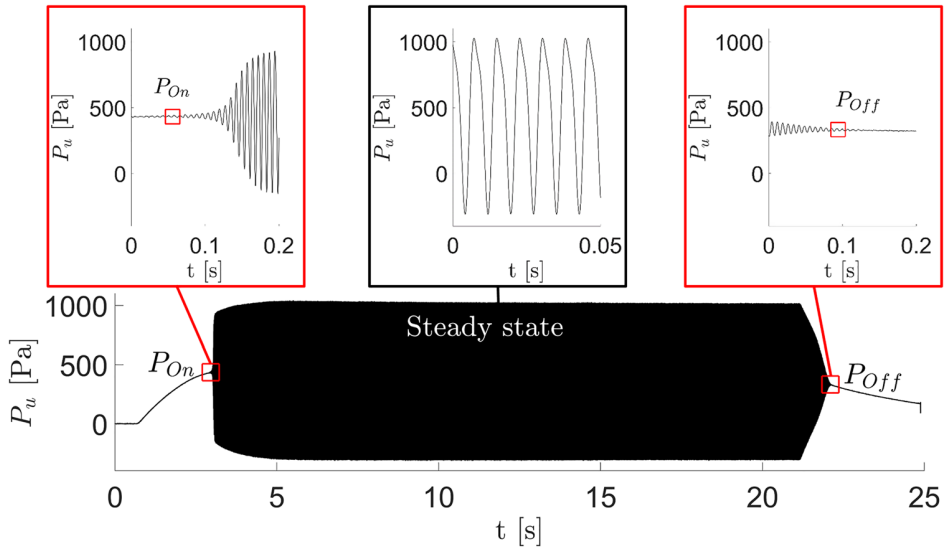

FIG. 6. (Color online) Measured upstream pressure time signal of $P_u(t)$ for the EPI replica with $\alpha = 0^\circ$. Oscillation onset POn and offset POff pressures are indicated (square) as is the steady state oscillatory signal portion ($\bar{P}_u \approx P_{On}$) used for analysis (5 s). For clarity, a zoom of $P_u(t)$ near oscillation onset (left), during steady state oscillation (middle), and near oscillation offset (right) is provided.

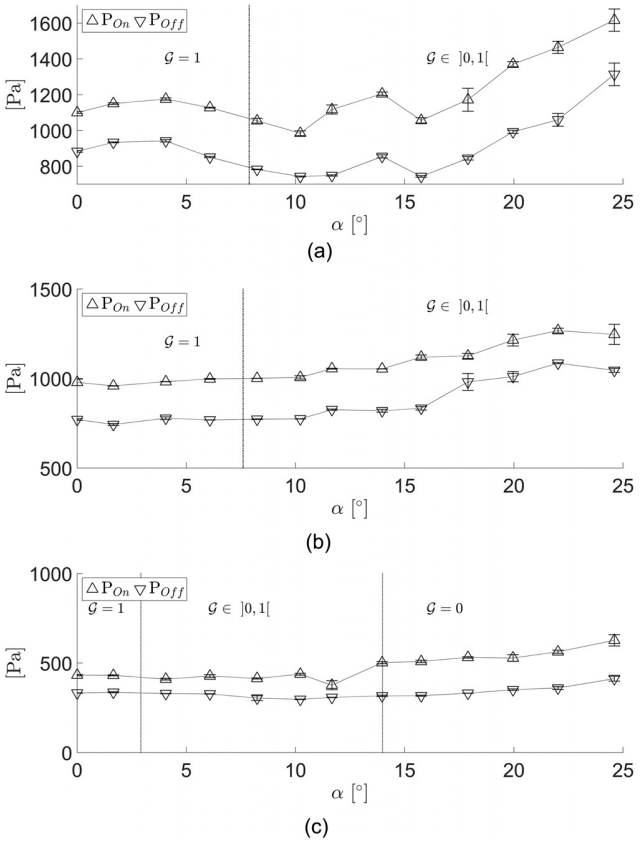

FIG. 7. Mean (symbols) and standard deviation (error bars) of onset POn and offset POff pressures as a function of asymmetry angle α: (a) M5, (b) MRI, and (c) EPI. Critical angles (vertical lines) indicate contact regime changes between $\mathcal{G} = 1$ (I), $\mathcal{G} \in]0, 1[$ (II), and $\mathcal{G} = 0$ (III), (a) M5, (b) MRI, (c) EPI.

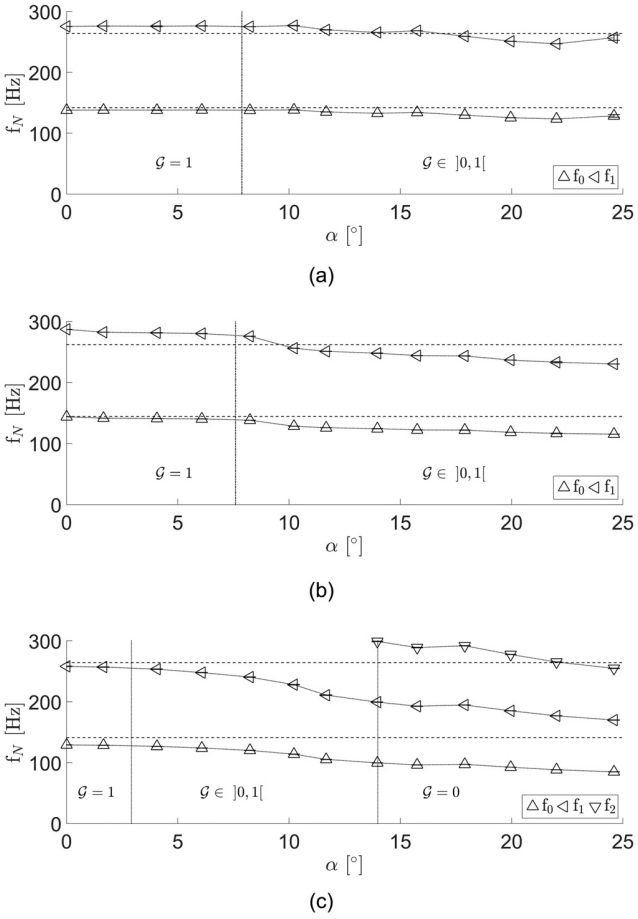

FIG. 8. Mean (symbols) and standard deviation (error bars) of harmonic frequencies (fN) at the phonation onset, as a function of asymmetry angle α: (a) M5, (b) MRI, and (c) EPI. Critical angles (vertical lines) indicate contact regime changes between $\mathcal{G} = 1$ (I), $\mathcal{G} \in]0, 1[$ (II), and $\mathcal{G} = 0$ (III). Horizontal dashed lines indicate mechanical resonance frequencies $f^M_{1,2}$, (a) M5, (b) MRI, (c) EPI.

observed that more realistic replicas (i.e., MRI and EPI) exhibit a more monotonic tendency than the M5 replica. For all replicas, hysteresis between the onset and offset pressures is observed as expected. The degree of hysteresis is only marginally affected by α in contact regimes I and II (all replicas: M5, MRI, and EPI), whereas it is reinforced in contact regime III (EPI replica only).

For symmetric angular configuration ($\alpha = 0°$), the detected oscillation frequencies f_0 and f_1 are located close to the first and second mechanical resonance frequencies given in Table III. This suggests that the auto-oscillation resulting from the fluid-structure interaction is aerodynamically driven. Thereafter, the fundamental frequency f_0 decreases monotonically with α. The overall decrease of f_0 relative to its value for symmetric configuration ($\alpha = 0°$) is quantified in Table V for all three replicas. It follows that the decrease is negligible ($< 3\%$) in contact regime I (full contact, $\mathcal{G} = 1$) and becomes more pronounced ($> 10\%$) in regimes II (partial contact, $\mathcal{G} \in]0, 1[$) and III (no contact, $\mathcal{G} = 0$). The second harmonic f_1 is detected for all replicas and all asymmetry angles α of regimes I and II. For the EPI replica, the third harmonic f_2 is detected for all α in regime III, indicating that the harmonic power increases with α.

The increased power of harmonics can be confirmed by the THD plotted in Fig. 9. For all replicas, the THD increases as the asymmetry angle α is increased. The increase is most prominent in contact regime II ($\mathcal{G} \in]0, 1[$) as it yields about 10 dB for the EPI replica and about 25 dB for the M5 and MRI replicas. The imprint of higher harmonics on the temporal waveform shape of steady state $P_u(t)$ for EPI is illustrated in Fig. 10 for $\alpha = 0°$ (few harmonics, low THD) and $\alpha = 20°$ (rich harmonic contents, high THD). The ratio between first and second harmonic powers $\mathcal{P}_{f_1}/\mathcal{P}_{f_0}$ is plotted in Fig. 11. The ratio increases with α toward 1 for all

TABLE IV. Minimum and maximum onset pressures relative [%] to the value for $\alpha = 0°$ and associated a [°].

	Minimum		Maximum	
Replica	[%]	[°]	[%]	[°]
M5	−10.5	10.2	46.9	24.6
MRI	−2.0	1.7	29.5	22.0
EPI	−12.9	11.7	45.0	24.6

https://doi.org/10.1121/10.0000742

TABLE V. Overall decrease of fundamental frequency f_0 relative [%] to the value for $\alpha = 0°$ in the full contact (I), partial contact (II), and no contact (III) regimes.

Replica	I	II	III
M5	0.3	−10.3	not measured
MRI	−2.4	−19.8	not measured
EPI	−0.5	−22.8	−34.2

replicas in regime II ($\mathcal{G} \in]0, 1[$), indicating that both harmonics contribute almost equally. Figure 12 shows that, for all replicas, increased THD is accompanied by a reduced SNR ratio of about 15 dB.

For all three replicas, angular asymmetry within contact regime I (full contact) showed only a minor influence on onset pressures P_{On}, oscillation frequencies f_0, THD, and SNR, which are close to those observed for symmetric angular configuration ($\alpha = 0°$). In contact regime II (up to $\alpha \leq 15°$), the THD and SNR start to deteriorate as α increases. For $\alpha > 15°$, all features (P_{On}, f_0, THD, and SNR) are affected by the angular asymmetry.

Some of our observations may elucidate medical findings reported on human patients having UVFP.[1] For instance, reduced SNR due to air leakage in contact regimes II and III through the glottal gap is consistent with a breathy voice description. Increased oscillation onset pressure P_{On} in contact regimes II and III may cause vocal fatigue (VFs constantly subjected to greater forces). The decrease in fundamental frequency f_0, on the other hand, does not follow the unnatural high-pitched voice described for UVFP. This might be due to several reasons such as the increased contribution of the observed higher harmonics to the perceived pitch, mechanical property changes in the paralyzed VF, which are not considered in the current work, or yet compensatory strategies involving supra-laryngeal structures of human speakers. These aspects need further investigation. In our studied range of asymmetry angles, aphonia (or oscillation death) could not be reproduced. Finally, it is noted from Fig. 4(c) that α-ranges, for which $h_A \leq 3$ mm (i.e., vertical level difference observed during human phonation[3]) extend up to contact regime II for all three replicas: $\alpha \leq 13°$ for EPI and $\alpha \leq 17°$ for both EPI and MRI. Therefore, partial contact (regime II) is of particular importance for phonation with UVFP.

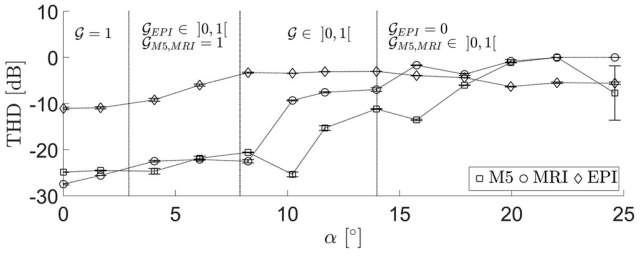

FIG. 9. Mean (symbols) and standard deviation (error bars) of THD (in dB) as a function of asymmetry angle α for all replicas. Critical angles (vertical lines) indicate contact regime changes between $\mathcal{G} = 1$ (I), $\mathcal{G} \in]0, 1[$ (II), and $\mathcal{G} = 0$ (III).

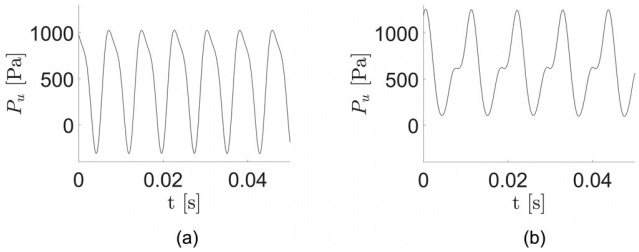

FIG. 10. Measured upstream pressure $P_u(t)$ for EPI steady state oscillation: (a) $\alpha = 0°$ and (b) $\alpha = 20°$. (a) Steady state, $\alpha = 0°$. (b) Steady state, $\alpha = 20°$.

IV. PARALLEL LEVEL DIFFERENCE ANALOGY FROM P_{ON}

In Refs. 4 and 5, a parallel level difference ΔE was imposed by varying the distance in the inferior-superior direction between both VFs while they remain parallel to the posterior-anterior axis. It follows that the glottal leakage due to parallel level difference ΔE is rectangular. This is in contrast to the triangular leakage area associated with angular asymmetry α in this study. Consequently, when imposing ΔE, only regime I (full contact) and regime III (no contact) occur for the parallel level difference. When imposing asymmetry angle α, on the other hand, partial contact (regime II) can also happen. Nevertheless, major tendencies observed for increasing asymmetry angle α (Section B), such as a decrease in fundamental frequency f_0 and overall increase in onset pressure P_{On}, have been also reported when parallel level difference ΔE was increased.[4,5] Therefore, a parallel level difference analogy $\Delta E(\alpha)$ is assessed expressing angular level difference, in terms of an equivalent parallel level difference, as $\Delta E(\alpha) \approx h_{l_A}(\alpha)$ with $h_{l_A}(\alpha) = A(\alpha)/l_A(\alpha)$ [i.e., the height of the rectangle obtained from glottal gap area $A(\alpha)$ and width $l_A(\alpha)$].

Using this analogy, the modeling approach outlined in Ref. 4, under the assumptions of small amplitude approximation of the VFs oscillation,[12] no acoustical coupling with sub- and supra-glottal systems and mechanical left-right VF symmetry, results in a theoretical expression of the oscillation onset threshold pressure P_{On} as a function of $h_{l_A}(\alpha)$:

$$P_{On}(h_{l_A}(\alpha)) = \frac{\tilde{w}\tilde{E}}{\left(\tilde{E} - h_{l_A}(\alpha)\right)^2}, \tag{7}$$

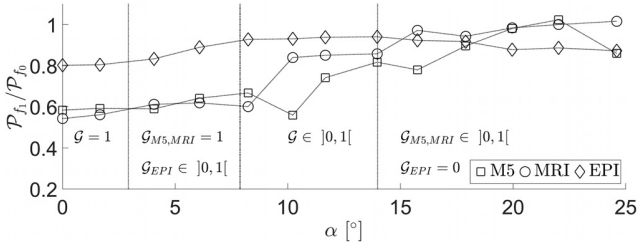

FIG. 11. Harmonics power ratio $\mathcal{P}_{f_1}/\mathcal{P}_{f_0}$ as a function of asymmetry angle α for M5, MRI, and EPI. Critical angles (vertical lines) indicate contact regime changes between $\mathcal{G} = 1$ (I), $\mathcal{G} \in]0, 1[$ (II), and $\mathcal{G} = 0$ (III).

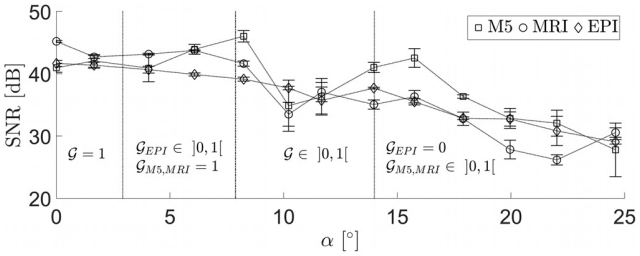

FIG. 12. Mean (symbols) and standard deviation (error bars) of SNR in (dB) as a function of asymmetry angle α for all replicas. Critical angles (vertical lines) indicate contact regime changes between $\mathcal{G} = 1$ (I), $\mathcal{G} \in]0, 1[$ (II), and $\mathcal{G} = 0$ (III).

with model parameter set $\{\tilde{w}, \tilde{E}\}$. The parameter $\tilde{w}$ accounts for mechanical damping per unit area, mucosal surface wave velocity, and pre-phonatory glottal half-width. The parameter $\tilde{E}$ corresponds to the largest VF thickness.

Fitted curves for $P_{On}(h_{l_A}(\alpha))$ using Eq. (7) and experimental data are shown in Fig. 13. The fit accuracy expressed by the coefficient of determination R^2 yields 89% for the M5 replica ($h_{l_A} \leq 2.9$ mm), 89% for the EPI replica ($h_{l_A} \leq 3.1$ mm), and 81% for the MRI replica ($h_{l_A} \leq 3.7$ mm). The VF thickness $\tilde{E}$ is estimated as 12 mm for M5, 26 mm for MRI, and 15 mm for EPI. Compared to the real values of $E \approx 10$ mm (see Table II), the estimates are of the same order of magnitude as the experimental measurements.

V. CONCLUSION

An experimental study is presented on the effect of angular level difference on the auto-oscillation for three mechanical VF replicas. Spectral features of upstream pressure (harmonic frequencies, THD, and SNR) as well as upstream threshold pressures (oscillation onset and offset) are analyzed. The same tendencies are observed for all three replicas. As the asymmetry angle α is increased so that VFs are no longer in full contact (contact regimes II and III), dynamics of the VF replica are clearly altered: SNR decreases, THD increases, oscillation threshold pressures increase, fundamental frequencies decrease, and higher harmonics emerge. Geometrical details of each VF replica determine the leakage area and critical asymmetry angles associated with a shift in contact regime. Expressions are given to quantify these features from geometrical VF parameters. Apart from the decrease in fundamental frequency, observed tendencies are in good agreement with those reported in clinical studies on vertical level difference. The same geometrical reasoning and expressions might be applied to characterize the glottal gap during phonation of patients with UVFP. Based on analogy to parallel level difference, a formula is proposed to describe the oscillation onset pressure as a function of the asymmetry angle.

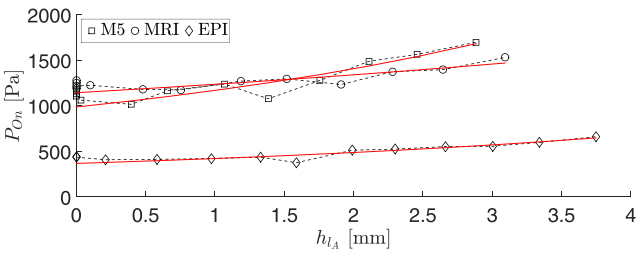

FIG. 13. (Color online) Measured (symbols) $P_{On}(h_{l_A}(\alpha))$ and predicted (full lines) using Eq. (7) for all replicas.

Currently, few measurements have been reported on level difference for UVFP. Various attempts have been recently made to measure three-dimensional *in vivo* geometry of the VFs (e.g., stereo endoscopy[24] and laser systems[25,26]). Such advanced measurements may eventually provide more precise information about the left-right angular asymmetry of patients with voice pathology. Geometrical expressions derived in this study [$A(\alpha)$ in Eq. (2), $l_A(\alpha)$ in Eq. (3), etc.] could be applied to characterize VF contact ($\mathcal{G}$ and regime) for patients. This study on the oscillation onset and voice quality features could be of great use as a reference for breathy voice, vocal fatigue, and other symptoms of voice disorders.

ACKNOWLEDGMENTS

This work was partly supported by the ArtSpeech project (ANR-15-CE23-0024), JSPS International Research Fellowship (Graduate School of Science, Ritsumeikan University, SP18205), and JSPS Grant-in-Aid for Scientific Research (Grant No. 19H01002). Authors thank T. Otsuka and Dr. K. Ishimura (Ritsumeikan University, Japan) for experimental support.

[1]C. Rosen and C. Simpson, *Operative Techniques in Laryngology* (Springer Verlag, Berlin, Germany, 2008), pp. 29–35.
[2]K. Hong and K. Jung, "Arytenoid appearance and vertical level difference between the paralyzed and innervated vocal cords," Laryngoscope **111**, 227–232 (2001).
[3]Y. Oyamada, E. Yumoto, K. Nakano, and H. Goto, "Asymmetry of the vocal folds in patients with vocal fold immobility," Arch. Otolaryngol. Head Neck Surg. **131**, 399–406 (2004).
[4]I. Tokuda and R. Shimamura, "Effect of level difference between left and right vocal folds on phonation: Physical experiment and theoretical study," J. Acoust. Soc. Am. **142**, 482–492 (2017).
[5]R. Shimamura and I. T. Tokuda, "Experimental study on level difference between left and right vocal folds," Acoust. Sci. and Tech. **38**, 264–267 (2017).
[6]K. Ishizaka and N. Isshiki, "Computer simulation of pathological vocal-cord vibration," J. Acoust. Soc. Am. **60**, 1193–1198 (1976).
[7]I. Steinecke and H. Herzel, "Bifurcations in an asymmetric vocal fold model," J. Acoust. Soc. Am. **97**, 1874–1881 (1995).
[8]J. Neubauer, P. Mergell, U. Eysholdt, and H. Herzel, "Spatio-temporal analysis of irregular vocal fold oscillations: Biphonation due to desynchronization of spatial modes," J. Acoust. Soc. Am. **110**, 3179–3192 (2001).
[9]Z. Zhang, "Vibration in a self-oscillating vocal fold model with left-right asymmetry in body-layer stiffness," J. Acoust. Soc. Am. **128**, EL279–EL285 (2010).
[10]Z. Zhang, J. Kreiman, and B. R. Gerratt, "Acoustic and perceptual effects of changes in body layer stiffness in symmetric and asymmetric vocal fold models," J. Acoust. Soc. Am. **133**, 453–462 (2013).
[11]J. C. Lucero, J. Schoentgen, J. Haas, P. Luizard, and X. Pelorson, "Self-entrainment of the right and left vocal fold oscillators," J. Acoust. Soc. Am. **137**, 2036–2046 (2015).
[12]I. R. Titze, "The physics of small-amplitude oscillation of the vocal folds," J. Acoust. Soc. Am. **83**, 1536–1552 (1988).
[13]D. G. Childers and C. K. Lee, "Vocal quality factors: Analysis, synthesis and perception," J. Acoust. Soc. Am. **90**, 2394–2410 (1991).

https://doi.org/10.1121/10.0000742

[14]J. P. Teixeira and P. O. Fernandes, "Jitter, shimmer and HNR classification within gender, tones and vowels in healthy voices," Procedia Technol. **16**, 1228–1237 (2014).
[15]B. Pickup and S. Thomson, "Flow-induced vibratory response of idealized versus magnetic resonance imaging-based synthetic vocal fold models," J. Acoust. Soc. Am. **128**, EL124–EL129 (2010).
[16]P. Murray and S. Thomson, "Synthetic, multi-layer, self-oscillating vocal fold model fabrication," J. Vis. Exp. **58**, e3498 (2011).
[17]P. Murray and S. Thomson, "Vibratory responses of synthetic, self-oscillating vocal fold models," J. Acoust. Soc. Am. **132**, 3428–3438 (2012).
[18]M. Hirano, S. Kurita, and T. Nakashima, *Vocal Fold Physiology: Contemporary Research and Clinical Issues* (College-Hill Press, London, UK, 1983), pp. 22–43.
[19]F. Alipour and I. Titze, "Elastic models of vocal fold tissues," J. Acoust. Soc. Am. **90**, 1326–1331 (1991).
[20]Y. Min, I. Titze, and F. Alipour, "Stress-strain response of the human vocal ligament," Ann. Otol. Rhinol. Laryngol. **104**, 563–569 (1995).
[21]R. Chan, M. Fu, L. Young, and N. Tirunagari, "Relative contributions of collagen and elastin to elasticity of the vocal fold under tension," Ann. Biomed. Eng. **35**, 1471–1483 (2007).
[22]R. Scherer, D. Shinwari, K. De Witt, C. Zhang, B. Kucinschi, and A. Afjeh, "Intraglottal pressure profiles for a symmetric and oblique glottis with a divergence angle of 10 degrees," J. Acoust. Soc. Am. **109**, 1616–1630 (2001).
[23]M. Zanartu and G. Galindo, "Modeling the effects of a posterior glottal opening on vocal fold dynamics with implications for vocal hyperfunction," J. Acoust. Soc. Am. **136**, 3262–3271 (2014).
[24]D. E. Sommer, I. T. Tokuda, S. D. Peterson, K.-I. Sakakibara, H. Imagawa, A. Yamauchi, T. Nito, T. Yamasoba, and N. Tayama, "Estimation of inferior-superior vocal fold kinematics from high-speed stereo endoscopic data *in vivo*," J. Acoust. Soc. Am. **136**, 3290–3300 (2014).
[25]G. Luegmair, D. D. Mehta, J. B. Kobler, and M. Döllinger, "Three-dimensional optical reconstruction of vocal fold kinematics using high-speed video with a laser projection system," IEEE Trans. Medical Imaging **34**, 2572–2582 (2015).
[26]M. Semmler, S. Kniesburges, V. Birk, A. Ziethe, P. Patel, and M. Döllinger, "3D reconstruction of human laryngeal dynamics based on endoscopic high-speed recordings," IEEE Trans. Medical Imaging **35** 1615–1624 (2016).